RSC Advances

PAPER

View Article Online
View Journal | View Issue

Cite this: *RSC Adv.*, 2023, **13**, 35240

Isatin-based benzyloxybenzene derivatives as monoamine oxidase inhibitors with neuroprotective effect targeting neurogenerative disease treatment†

Feba Benny,‡[a] Jong Min Oh,‡[b] Sunil Kumar,[a] Mohamed A. Abdelgawad,[c] Mohammed M. Ghoneim,[d] Mohamed Sadek Abdel-Bakky,[e] Neelima Kukerti,[f] Jobin Jose,[g] Hoon Kim *[b] and Bijo Mathew *[a]

Eighteen isatin-based benzyloxybenzaldehyde derivatives from three subseries, **ISB**, **ISFB**, and **ISBB**, were synthesized and their ability to inhibit monoamine oxidase (MAO) was evaluated. The inhibitory activity of all synthesized compounds was found to be more profound against MAO-B than MAO-A. Compound **ISB1** most potently inhibited MAO-B with an IC_{50} of 0.124 ± 0.007 μM, ensued by **ISFB1** (IC_{50} = 0.135 ± 0.002 μM). Compound **ISFB1** most potently inhibited MAO-A with an IC_{50} of 0.678 ± 0.006 μM, ensued by **ISBB3** (IC_{50} = 0.731 ± 0.028 μM), and had the highest selectivity index (SI) value (55.03). The three sub-parental compounds, **ISB1**, **ISFB1**, and **ISBB1**, had higher MAO-B inhibition than the other derivatives, indicating that the substitutions of the 5-H in the A-ring of isatin diminished the inhibition of MAO-A and MAO-B. Among these, **ISB1** (*para*-benzyloxy group in the B-ring) displayed more significant MAO-B inhibition when compared to **ISBB1** (*meta*-benzyloxy group in the B-ring). **ISB1** and **ISFB1** were identified to be competitive and reversible MAO-B inhibitors, having K_i values of 0.055 ± 0.010, and 0.069 ± 0.025 μM, respectively. Furthermore, in the parallel artificial membrane penetration assay, **ISB1** and **ISFB1** traversed the blood–brain barrier in the *in vitro* condition. Additionally, the current study found that **ISB1** decreased rotenone-induced cell death in SH-SY5Y neuroblastoma cells. In docking and simulation studies, the hydrogen bonding formed by the imino nitrogen in **ISB1** and the pi–pi stacking interaction of the phenyl ring in isatin significantly aided in the protein–ligand complex's stability, effectively inhibiting MAO-B. According to these observations, the MAO-B inhibitors **ISB1** and **ISFB1** were potent, selective, and reversible, making them conceivable therapies for neurological diseases.

Received 16th October 2023
Accepted 26th November 2023

DOI: 10.1039/d3ra07035b

rsc.li/rsc-advances

Introduction

Parkinson's disease (PD) is a progressive neurological condition associated with motor impairment, with approximately 2% of people over 65 years of age affected by this condition worldwide.[1,2] Dopamine (DA) levels in the putamen and caudate nucleus are reduced in people with PD. Dopaminergic neurons are selectively reduced in the substantia nigra pars compacta and cytoplasm. The symptoms of this illness include Lewy bodies with aggregated α-synuclein.[3–5] Although the exact trigger of PD is unknown, numerous studies reveal that, besides the DA depletion, additional factors such as neuroinflammation, protein aggregation, a lack of support from neurotrophic factors, oxidative stress, dysregulation of the autophagy-lysosomal pathway, and mitochondrial dysfunction contribute to the advancement of the disease. The 1960s marked the introduction of monoamine oxidase (MAO) inhibitors, but small biogenic molecules containing 3,4-dihydroxyphenylalanine (L-DOPA) have been used to treat PD symptoms

[a]*Department of Pharmaceutical Chemistry, Amrita School of Pharmacy, Amrita Vishwa Vidyapeetham, AIMS Health Sciences Campus, Kochi, 682041, India. E-mail: febacbenny@gmail.com; solankimedchem@gmail.com; bijovilaventgu@gmail.com; bijomathew@aims.amrita.edu*

[b]*Department of Pharmacy, Research Institute of Life Pharmaceutical Sciences, Sunchon National University, Suncheon 57922, Republic of Korea. E-mail: ddazzo005@naver.com; hoon@sunchon.ac.kr*

[c]*Department of Pharmaceutical Chemistry, College of Pharmacy, Jouf University, Sakaka 72341, Saudi Arabia. E-mail: mhmdgwd@ju.edu.sa*

[d]*Department of Pharmacy Practice, College of Pharmacy, AlMaarefa University, Ad Diriyah 13713, Saudi Arabia. E-mail: mghoneim@mcst.edu.sa*

[e]*Department of Pharmacology and Toxicology, College of Pharmacy, Qassim University, Buraydah 51452, Saudi Arabia. E-mail: abdelbakkym@yahoo.com*

[f]*School of Pharmacy, Graphic Era Hill University, Dehradun, Uttarakhand 248002, India. E-mail: nkukreti@gehu.ac.in*

[g]*Department of Pharmaceutics, NGSM Institute of Pharmaceutical Science, NITTE University, Mangalore, Karnataka 575018, India. E-mail: jjmattam07@gmail.com*

† Electronic supplementary information (ESI) available: TLC, HPLC, ^{1}H-, ^{13}C-NMR and MS spectra of all compounds. See DOI: https://doi.org/10.1039/d3ra07035b

‡ Authors contributed equally to this work.

since the end of the 1950s.[6,7] MAO-B inhibitors have been widely employed for the symptomatic treatment of PD,[8] because they reduce the rate of oxidative deamination catalyzed by MAO-B and subsequently decrease the formation of reactive oxygen species (ROS).[9,10] MAO-B inhibitors have remarkable efficacy and safety when used in the early stages of PD and as adjunctive therapy for advanced illnesses.[8] Dopamine is released into the synaptic cleft and absorbed by glial cells, where it is metabolized by MAO-B. An age-related increase in glial cells has been linked to elevated MAO-B activity in neurodegenerative disorders.[11–13] MAO-B inhibitors suppress brain MAO-B activity, inhibit dopamine catabolism, improve dopamine signaling, and elevate synaptic dopamine levels.[14,15] Numerous studies have suggested that irreversible MAO-B inhibitors, such as rasagiline and selegiline, can successfully fix the motor dysfunction and prevent dopamine degradation in PD patients. However, the target disruption, a longer half-life, *de novo* formation of MAO enzyme in the human brain, decreased sensitivity to ADME testing and immunogenicity of the MAO-B-inhibitor adduct include the pitfalls of irreversible MAO-B inhibitors.[16–18] These characteristics aided in creating effective and reversible MAO-B inhibitors for treating PD. Recently, the European Union (EU) and the US Food and Drug Administration (USFDA) approved safinamide, which is a reversible MAO-B inhibitor to combat mid- to late-stage PD.[19–21]

A considerable number of reports have been published on the synthesis, biological assessment, and formulation of MAO inhibitors. Most drugs frequently contain specific pharmacophores with strong MAO-B inhibitory action and selectivity. Such pharmacophores include compounds that contain benzyloxy groups with strong MAO inhibitory effects.[22–24] Benzyloxy substituents have been reported as selective MAO-B inhibitors in a series of oxadiazon derivatives.[25] A series of compounds are reported to have improved molecular hydrophobicity as a result of the benzyloxy group attached to the fifth position of the indole ring, which is consistent with the environment of the active site and is crucial for MAO-B selectivity.[26] Studies have confirmed that a benzyloxy group, which is substituted at the indole ring's fifth position, is found crucial to establish the selectivity of MAO-B inhibitory activity.[27,28] Safinamide is the first anti-Parkinson's medication to be recognized in the last 10 years that also inhibits glutamate release and the reuptake of DA and serotonin. Early anti-Parkinson's medications include selegiline and rasagiline, of which selegiline has a reversible effect and good pharmacokinetic profile and a bioavailability[29] of about 95%. Safinamide, on the other hand, has a distinctive structural makeup with an apparent benzyloxy pharmacophore on the phenyl ring and an aminoamide in the proper para position.[30] It has been reported that safinamide[31,32] and indolalkylamines[33,34] contain benzyloxy groups and that halogenation of the benzyloxy pharmacophore of the chalcone framework could enhance MAO-B inhibition.[35]

Isatin is an indoledione, a pharmacologically active molecule that is the 2,3-diketo derivative of indole.[36,37] Derivatives of isatin are widely known for their effective blood–brain barrier (BBB) penetration as well as their selectively reversible MAO-B inhibitory action.[38] Human MAO-A and MAO-B are both reversibly inhibited by isatin, with K_i values of 15 μM and 3 μM, respectively.[39,40] Isatin is an extremely reactive compound that has been employed as both an electrophile and a nucleophile in synthetic chemistry. Isatin derivatives possess several biological properties, including anticancer,[41–43] antibiotic,[44] antidepressant, anxiogenic, sedative, anticonvulsant,[45,46] antibacterial, antidiabetic,[47] carboxyesterase,[48,49] anti-platelet, and anti-HIV[50] effects. The most prevalent electrophilic reaction of isatin is a nucleophilic addition to the third-position keto group. There have been many published investigations on the synthesis of isatin spiro analogues at the C-3 position.[28]

We developed a versatile chemical methodology (Fig. 1) that employs the molecular hybridization of isatin and safinamide to produce benzyloxy isatin hydrazones. Isatin is an endogenous MAO inhibitor, and substituting C-3 position with the lipophilic group markedly enhances the MAO-B inhibition.[39,40] Main pharmacophore of the FDA-approved drug safinamide is 3-fluoro-(benzyl)-benzyloxy unit. Our design was focused on generating a hybrid class of compounds with these pharmacophores to produce a novel class of chemical entities in the category of MAO inhibitors. A hydrazone linker was used to link the isatin scaffold to a benzyloxy pharmacophore. This chemistry uses a microwave-mediated attachment of an isatin hydrazone linker to different benzyloxy benzaldehyde functionalities catalyzed by glacial acetic acid. Isatin hydrazone-based derivatives are selective, reversible, and effective inhibitors of MAO-B.[51] According to earlier research, all isatin hydrazone-based inhibitors bind to both the substrate (Ile168, Tyr60, Tyr398, Cys172, Phe343, Tyr435, and Gln206) and entrance (Tyr326, Leu171, and Ile199) cavities, which is similar to the behavior of the reference MAO-B inhibitor, safinamide.[28,51,52]

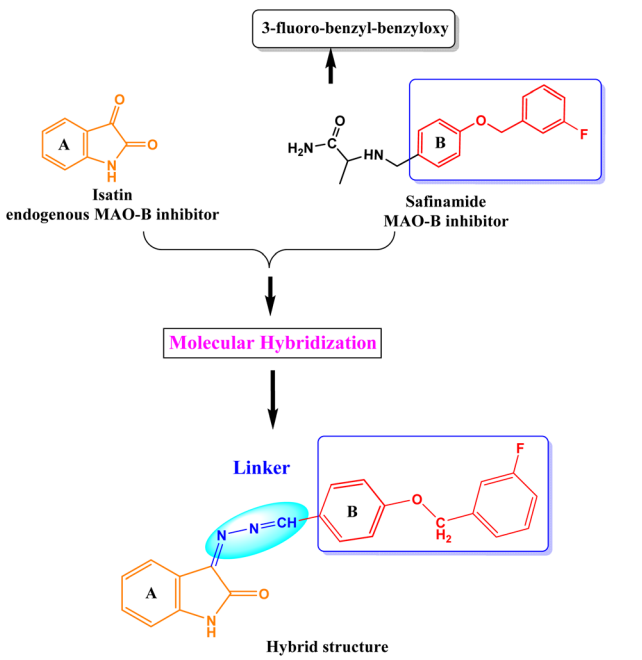

Fig. 1 Design strategy of benzyloxy isatin hydrazones.

Results and discussion

Chemistry

With various substituted isatin hydrazides and *para*-substituted benzyloxy benzaldehyde, the isatin-based benzyloxy-benzaldehyde derivatives were synthesized in a microwave reactor (Monowave 50, Anton Paar, Graz, Austria) by means of a nucleophilic addition reaction (Fig. 2). Using ^{1}H NMR, ^{13}C NMR (Bruker Advance Neo 500 MHz NMR spectrometer, Billerica, MA, USA), mass spectroscopy (Waters Xevo G2-XS QTOF, Milford, MA, USA), and HPLC (Shimadzu Prominence-i LC-2030C 3D Plus, Ramsey, MN, USA), structures of all final derivatives were investigated. Isatin with NH atom for proton occurs inside the 10.66–11.00 ppm di-shielded region. Benzyloxy–CH_2 atom shielded proton in 5.23–5.33 ppm. The extensively di-shielded area 163–164.24 ppm included sp^2 carbon of carbonyl carbon of isatin. In the di-shielded region of 159–163 ppm, C–F coupling also occurred (source data supporting).†

Inhibition studies of MAO-B and MAO-A

There were 18 compounds in this series, divided into three subseries and three sub-parental compounds: **ISB1**, **ISFB1**, and **ISBB1**. In this series, all of the compounds displayed more profound MAO-B inhibitory actions than MAO-A (Table 1). Compound **ISB1** most potently inhibited MAO-B, with an IC_{50} = 0.124 μM, followed by **ISFB1** (IC_{50} = 0.135 μM) (Table 1). These IC_{50} values were lower than methylthiosemicarbazone **SM5** (IC_{50} = 5.48 μM) and piperazine-substituted chalcones **PC10** and **PC11** (IC_{50} = 0.65 and 0.71 μM, respectively)[53] but higher than benzyloxy pharmacophore **B10** (IC_{50} = 0.067 μM).[54] Compound **ISFB1** inhibited MAO-A with an IC_{50} = 0.678 μM, followed by **ISBB3** (IC_{50} = 0.731 μM). The selectivity index (SI) for compounds **ISB1** and **ISFB1** were 55.03 and 5.02, respectively, for MAO-B compared to MAO-A, indicating that these compounds were selective MAO-B inhibitors (Table 1).

The structure–activity relationship (SAR) for the **ISB** derivatives showed that **ISB1** (5-H in A-ring of isatin and *para*-benzyloxy group in B-ring) had 52.93- to 142.11-times higher MAO-B inhibition than other **ISB** derivatives with the substituents of –H > –H_3C > –Cl > –F > –Br > –H_3CO at the 5-position in the A-ring. In the **ISFB** derivatives, **ISFB1** (5-H in A-ring of isatin and *para*-benzyloxy group containing *meta*-F in B-ring) had 8.81- to 153.84-times higher MAO-B inhibition than other **ISFB** derivatives with the substituents of –H > –F > –H_3C > –H_3CO > –Br > Cl at 5-position in the A-ring. Among the **ISBB** derivatives, **ISBB1** (5-H in the A-ring and *meta*-benzyloxy group in the B-ring) showed 1.12- to 28.07-times higher MAO-B inhibition than the other **ISBB** derivatives with –H > –F > –Cl > –Br > –H_3CO > –H_3C at the 5-position in the A-ring. When we compared the B-ring, the B-ring at the *para*-position (**ISB1**, IC_{50} = 0.124 μM) had higher MAO-B inhibition than that in the *meta*-position (**ISBB1**, IC_{50} = 0.540 μM), and MAO-B inhibition increased in order by –H **ISB1** > –F (**ISFB1**, IC_{50} = 0.135 μM). Overall, most compounds with –H substituents showed high MAO-B inhibition (Fig. 3 and Table 1). Collectively, the basic structures **ISB1**, **ISFB1**, and **ISBB1** with 5-H in the A-ring of isatin showed higher MAO-B inhibition than the other derivatives, suggesting that the substitution of the –H group of the A-ring contributed to a decrease in MAO-B inhibition. Among these, **ISB1** (*para*-benzyloxy group in the B-ring) showed higher MAO-B inhibition than **ISBB1** (*meta*-benzyloxy group in the B-ring). However, three sub-parental compounds, **ISB1**, **ISFB1**, and **ISBB1** (5-H substituent in the A-ring) displayed potent MAO-A inhibition, with IC_{50} values of 6.824, 0.678, and 1.570 μM, respectively. In addition, **ISBB3** (5-F in the A-ring and *meta*-benzyloxy group in the B-ring) showed high inhibitory activity (IC_{50} = 0.731 μM). In each subseries, the substitution of 5-H in the A-ring with other groups generally decreased MAO-A inhibition (Fig. 3 and Table 1). According to these results, **ISB1** and **ISFB1** were strong and selective MAO-B inhibitors.

Reversibility studies

Using the dialysis approach, the reversibility of inhibition of the **ISB** series was evaluated using concentrations that were ~2.0 times their respective IC_{50} values for **ISB1** and **ISFB1** (0.24 and 0.28 μM, respectively). Recovery patterns were determined by comparing the undialyzed (A_U) and dialyzed (A_D) relative

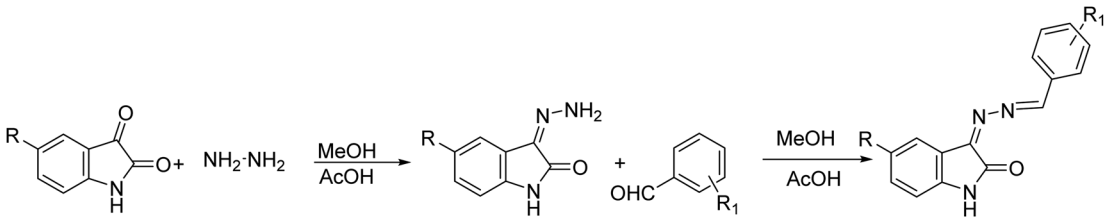

R	Code	R_1	Code	R_1	Code	R_1
-H	**ISB1**	4- benzyloxy	**ISFB1**	4-(-3-fluoro-benzyloxy)	**ISBB1**	3-benzyloxy
-Br	**ISB2**	4- benzyloxy	**ISFB2**	4-(-3-fluoro-benzyloxy)	**ISBB2**	3-benzyloxy
-F	**ISB3**	4- benzyloxy	**ISFB3**	4-(-3-fluoro-benzyloxy)	**ISBB3**	3-benzyloxy
-Cl	**ISB4**	4- benzyloxy	**ISFB4**	4-(-3-fluoro-benzyloxy)	**ISBB4**	3-benyzloxy
-OCH_3	**ISB5**	4- benzyloxy	**ISFB5**	4-(-3-fluoro-benzyloxy)	**ISBB5**	3-benzyloxy
-CH_3	**ISB6**	4- benzyloxy	**ISFB6**	4-(-3-fluoro-benzyloxy)	**ISBB6**	3-benzyloxy

Fig. 2 Synthesis of ISB, ISFB, and ISBB compounds.

Table 1 Inhibition of MAO-A and MAO-B by the 18 compounds of ISB series[a]

	Residual activity at 10 μM (%)		IC_{50} (μM)		
Compound	MAO-A	MAO-B	MAO-A	MAO-B	SI[b]
ISB1	38.78 ± 0.25	−8.77 ± 0.14	6.824 ± 0.049	0.124 ± 0.007	55.03
ISB2	87.76 ± 1.11	64.91 ± 1.24	>40	14.182 ± 0.250	>2.82
ISB3	74.49 ± 0.95	59.65 ± 1.11	>40	13.943 ± 0.204	>2.87
ISB4	84.69 ± 1.55	54.39 ± 2.01	>40	9.764 ± 1.349	>4.10
ISB5	85.71 ± 2.04	66.67 ± 1.35	>40	17.622 ± 0.202	>2.27
ISB6	89.80 ± 1.12	40.35 ± 0.99	>40	6.563 ± 0.206	>6.09
ISFB1	4.17 ± 0.32	−3.03 ± 0.24	0.678 ± 0.006	0.135 ± 0.002	5.02
ISFB2	88.54 ± 1.38	57.58 ± 1.10	>40	16.043 ± 0.308	>2.49
ISFB3	53.13 ± 0.44	24.50 ± 1.03	10.937 ± 0.220	1.189 ± 0.362	9.20
ISFB4	84.38 ± 1.24	63.64 ± 0.15	>40	20.768 ± 0.027	>1.93
ISFB5	87.50 ± 1.88	50.00 ± 0.38	>40	8.986 ± 0.079	>4.45
ISFB6	84.38 ± 1.52	30.30 ± 0.77	>40	4.100 ± 0.311	>9.76
ISBB1	4.84 ± 1.61	1.99 ± 0.86	1.570 ± 0.048	0.540 ± 0.029	2.91
ISBB2	81.52 ± 1.64	46.88 ± 0.88	>40	8.127 ± 0.383	>4.92
ISBB3	35.87 ± 1.02	29.69 ± 0.54	0.731 ± 0.028	0.607 ± 0.011	1.20
ISBB4	73.91 ± 0.04	40.63 ± 0.63	>40	6.058 ± 0.318	>6.60
ISBB5	58.70 ± 0.29	48.44 ± 0.44	11.054 ± 0.060	12.061 ± 3.567	0.92
ISBB6	65.22 ± 0.87	39.06 ± 0.21	14.422 ± 0.670	15.157 ± 0.419	0.95
Toloxatone			1.080 ± 0.025	—	
Lazabemide			—	0.110 ± 0.016	
Clorgyline			0.007 ± 0.0007	—	
Pargyline			—	0.140 ± 0.006	

[a] Results are the means ± standard errors of duplicate or triplicate experiments. [b] Selectivity index (SI) values are expressed for MAO-B compared to MAO-A.

activities. Compounds **ISB1** and **ISFB1** recovered from 31.61% to 83.77% and from 31.42% to 79.32%, respectively (Fig. 4). The compounds' recovery values were comparable to those of lazabemide (from 36.30% to 89.00%) and contrary to those of pargyline (from 33.55% to 30.46%). These findings demonstrated **ISB1** and **ISFB1** were reversible MAO-B inhibitors.

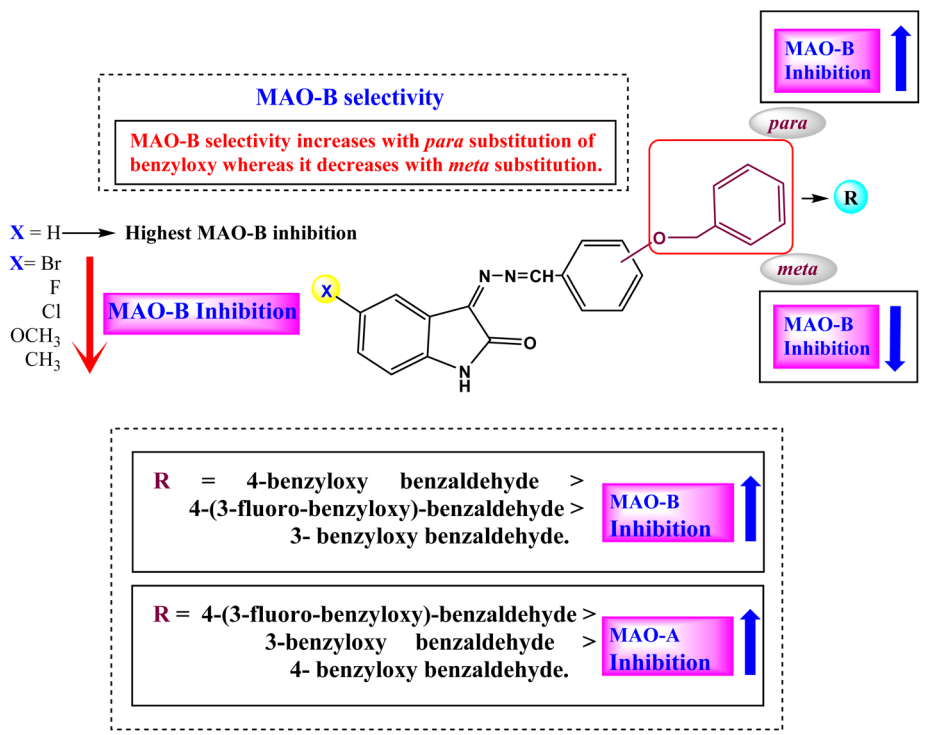

Fig. 3 Structure–activity relationships (SARs) of benzyloxybenzaldehyde derivatives.

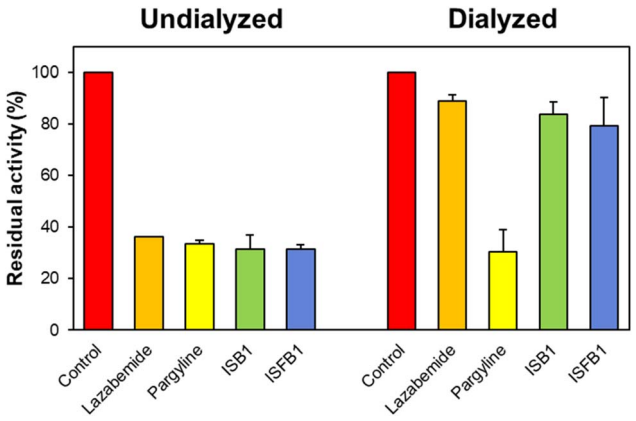

Fig. 4 Recovery of MAO-B inhibition by **ISB1** and **ISFB1** using dialysis experiments. The concentrations of **ISB1** and **ISFB1** were ~2.0-times of their IC_{50} values (0.24 and 0.28 μM, respectively). After 30 min preincubation, the mixtures were dialyzed for 6 h with two buffer changes.

Enzyme kinetics

The enzyme kinetics of MAO-B and the inhibition of five concentrations of benzylamine as a substrate and three inhibitor concentrations were analyzed. Lineweaver–Burk plots illustrated that **ISB1** and **ISFB1** appeared to be competitive MAO-B inhibitors (Fig. 5A and C). Secondary plots revealed that the K_i values were 0.055 ± 0.010 and 0.069 ± 0.025 μM, respectively, for **ISB1** and **ISFB1** (Fig. 5B and D). These results suggested that **ISB1** and **ISFB1** are competitive inhibitors of MAO-B.

PAMPA for BBB permeation study

PAMPA revealed that the central nervous system (CNS) bioavailability and permeability of the benzyloxy isatin hydrazones (**ISB1** and **ISFB1**) were significant, with Pe values higher than 4.0×10^{-6} cm s^{-1} (Table 2). Brain penetration is an important requirement for the effective delivery of CNS medications. The PAMPA-BBB was implemented in the present study to evaluate the brain penetration of all derivatives. Using the equation and the compound's effective permeability, the rate of permeation was computed (log Pe). Molecules were categorized as potentially non-BBB permeable (CNS−), if their Pe value was less than 2.0×10^{-6} cm s^{-1} and as potentially permeable (CNS+), if their Pe value was greater than 4.0×10^{-6} cm s^{-1}.

Effect of ISB1 on rotenone-induced cell viability

SH-SY5Y-human bone marrow neuroblastoma cell line was supplied from National Center for Cell Science (NCCS), Pune,

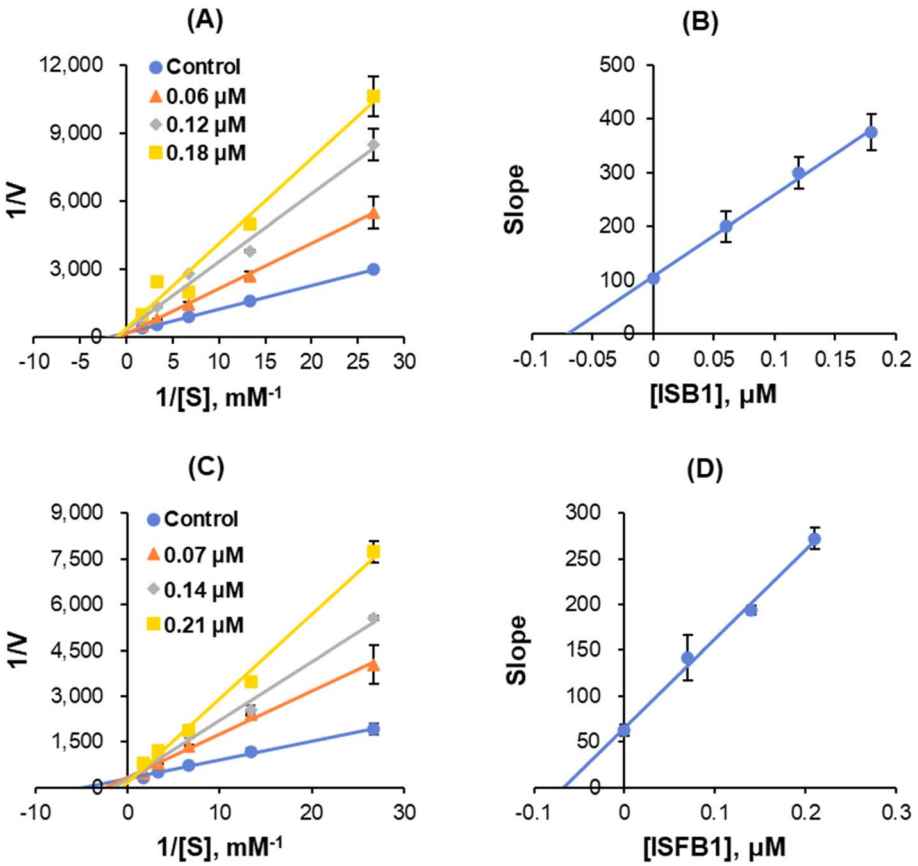

Fig. 5 Lineweaver–Burk plots for MAO-B inhibition (A and C, respectively), and respective secondary plots of the slopes *vs.* inhibitor concentrations (B and D, respectively) after **ISB1** and **ISFB1** treatment. The experiments were conducted using five concentrations of benzylamine as a substrate and at three different inhibitor concentrations.

Table 2 BBB assay of key benzyloxy chalcone compounds using the PAMPA method[a]

Compound	Experimental Pe ($\times 10^{-6}$ cm s^{-1})	Prediction
ISB1	4.93 ± 0.13	CNS+
ISFB1	4.09 ± 0.24	CNS+
Selegiline	5.69 ± 0.04	CNS+

[a] Pe (10^{-6} cm s^{-1}) > 4.00: CNS+ (high permeation).

Table 3 XP docking scores of promising compounds to the MAO-B (2V5Z) active sites

Compound	Docking score (kcal mol^{-1})
ISB1	−10.413
ISFB1	−9.370
Safinamide	−11.029

India. MTT assay test was used to determine neuroprotective effect of **ISB1** on rotenone-induced SH-SY5Y cells. **ISB1** increased cell viability in a dose-dependent manner for rotenone-treated SH-SY5Y cells (Fig. 6a). The cell viability was increased from about 50% at 1.5 μg ml^{-1} to 85.59% at 25 μg ml^{-1} of **ISB1**. The fundamental morphological changes of the cells on each concentration were observed by direct microscopic method (Fig. 6b).

Molecular docking

According to the results of enzyme assays, **ISB1** and **ISFB1** were determined to be the most effective and selective analogues of the series studied against human MAO-B enzymes. Thus, docking analyses were conducted to examine the binding mechanisms of compounds **ISB1** and **ISFB1** and to evaluate the effects of structural modifications on the MAO-B inhibitory activity of these compounds. The X-ray crystal structure of human MAO-B was found using the Protein Data Bank (PDB ID:2V5Z). **ISB1** and **ISFB1** had substantial docking scores for MAO-B, corroborating the findings of the enzyme activity assay and implying the selectivity for MAO-B (Table 3). **ISB1** had a docking score of −10.413 (XP Glide Score) for MAO-B. Fig. 7A displays the binding interactions between compound **ISB1** and MAO-B. The docking poses of hMAO-B displayed that the NH group of isatin was linked to Cys172 through a water molecule (2.15 Å) *via* hydrogen bonding. **ISB1** makes polar contact with Gln206, while the Tyr398, Tyr435, Phe343, Tyr60, Tyr326, Ile316, Trp119, Leu164, Ala165, and Leu171 amino acid side chains interacted hydrophobically with **ISB1**. As neither of the other compounds displayed a comparable interaction, it was assumed that this interaction was crucial for **ISB1** and would help to explain its stronger inhibitory effect. Thus, the presence of hydrogen bonding interactions between the –NH of isatin and Cys172 may significantly influence its biological activity. Compound **ISFB1** had a docking score of 9.370 (XP Glide Score) for MAO-B. Fig. 7B displays the interactions between compound **ISFB1** and MAO-B, which illustrates that the aromatic benzene ring of isatin in **ISFB1** was extended to hydrophobic residues

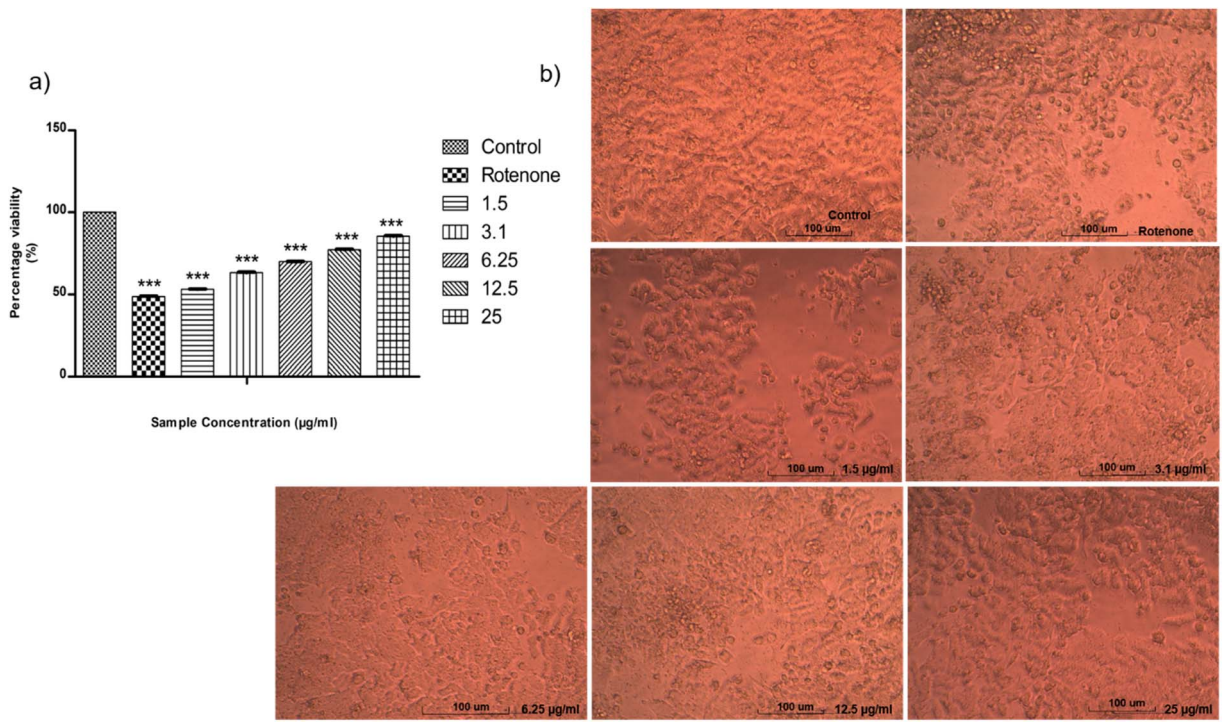

Fig. 6 (a) Graphical representation depicting the neuroprotective effect of ISB1 on SH-SY5Y cells by MTT assay. Co-treatment with ISB1 attenuated vulnerability of SH-SY5Y to rotenone. (b) The morphology changes of the cells.

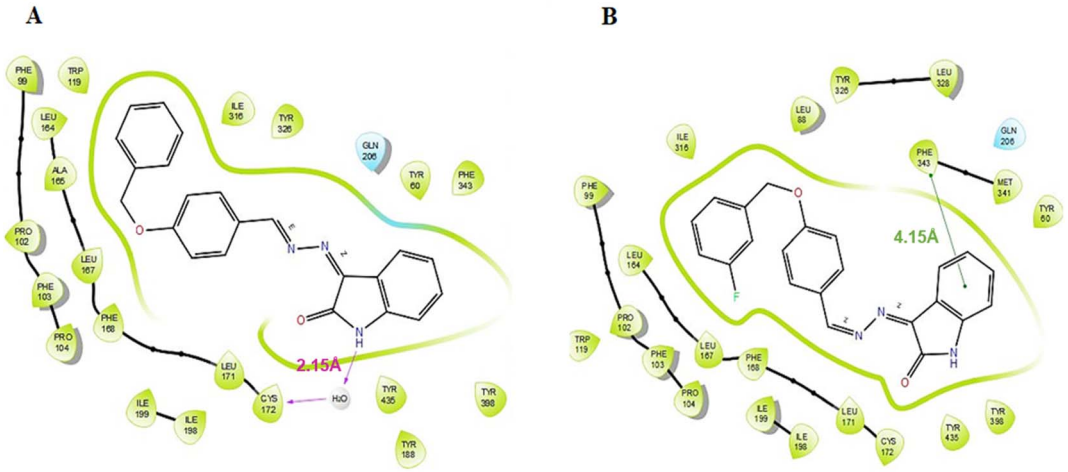

Fig. 7 Binding interactions of compounds **ISB1** (A) and **ISBF1** (B) to the active site of the MAO-B (PDB ID 2V5Z).

and engaged in π–π stacking with Phe343 (4.15 Å) and that **ISFB1** made polar contact with Gln206. The binding modalities of the novel compounds in the 2V5Z complex were predicted using hydrophobic interactions established with the adjacent amino acids compared to the reversible monoamine oxidase inhibitor, safinamide.

MD simulation

Since MD provides a single snapshot of the interaction between a protein and its ligands, it could possibly be used to describe all biological systems as dynamic networks of molecular interactions. To sample all of the conformations that this complex might acquire in a solvated state, we employed an explicit water model to simulate the dynamic behavior of the docked **ISB1**-MAO-B complex for a period of 100 ns. The main objective was to keep the ligand occupied in the substrate-binding pocket of the MAO-B enzyme and to conserve the major interactions found in the best docked posture throughout the MD simulation.

RMSD

The RMSD value obtained from the MD simulation trajectory is one of the crucial metrics that demonstrates fluctuations in the structural conformation of the protein backbone over time during system equilibration; low and consistent RMSD values signify the stability of a protein structure. The RMSD of MAO-B with **ISB1** ranged from 2.00 and 3.60 Å, with the complex's RMSD value reported at 2.28 Å on average. In the simulation trajectory, the ligand RMSD displayed little change and was estimated to be between 40 and 60 ns. Thereafter, the simulation's remaining frame marked gradual convergence. Analysis of the trajectory revealed that the phenyl ring of the free-moving benzyloxy moiety was the main cause of this fluctuation. Overall, there was little departure from the docked stance in the **ISB1**-hMAO-B docked complex (Fig. 8).

In addition to RMSD, the RMSF value of a protein is widely used to assess ligand-induced variations in the protein's internal chains. The RMSF renders details on the flexibility and mobility of specific amino acids. A lower RMSF value indicates that the residue is less flexible and mobile. In ligand–protein interactions, the ligand establishes stronger binding with the protein when the RMSF value is low at the active site residues. Low values reflect the existence of secondary structures, including sheets and helices, which determine structural stability. The presence of twists, loops, terminal ends, and loose bonding, on the other hand, is represented by greater RMSF values (peaks), which implies structural flexibility.[55–60] Thus, the protein RMSF plot analysis provided details of the flexible areas of the protein. Our analysis found that **ISB1** made contact with 24 amino acids of the hMAO-B protein, which included His90 (0.715 Å), Gly101 (1.212 Å), Pro102 (1.16 Å), Phe103 (1.02 Å), Pro 104 (0.892 Å), His 115 (0.832 Å), Trp 119 (0.699 Å), Leu 164 (0.803 Å), Leu 167 (0.735 Å), Phe 168 (0.701 Å), Leu 171 (0.703 Å), Cys 172 (0.778 Å), Tyr 188 (0.542 Å), Ile 198 (0.588 Å), Ile 199 (0.716 Å), Thr 201 (0.832 Å), Gln 206 (0.592 Å), Ile 316 (0.666 Å), Tyr 326 (0.523 Å), Leu 328 (0.627 Å), Phe 343 (0.474 Å), Leu 345 (0.677 Å), Tyr398 (0.475 Å), and Tyr 435 (0.457 Å). The catalytic pocket residues displayed considerably less fluctuation than other residues, with the exception of the terminal 498–502 residues near the N-terminus, implying that the conformation of the residue remained reasonably stable during the simulation (Fig. 8).

Materials and methods

Chemical synthesis

Isatin hydrazone (1 equivalent) was synthesized using the chemical reaction of isatin substituted with hydrazine hydrate (2.5 equivalent) and glacial acetic acid under microwave radiation using methanol as a solvent. The mixture of isatin hydrazone (1 equivalent) and a substituted benzyloxy benzaldehyde (1 equivalent) was dissolved in 7.5 mL methanol using glacial acetic acid as a catalyst, and placed in the microwave reactor for 10 min at 120 °C. The precipitate obtained as a solid product was then filtered. The mixture was washed with methanol and

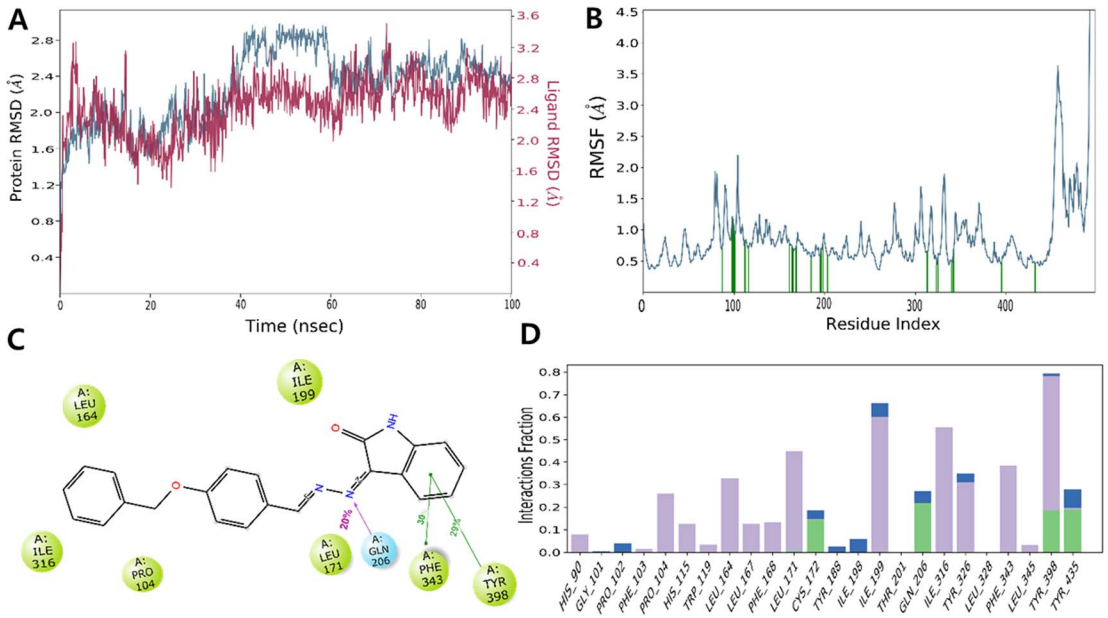

Fig. 8 Molecular docking (MD) simulation analysis of **ISB1**-MAO-B complex. Root-mean-square deviation (RMSD) (A) and root-mean-square fluctuation (RMSF) of various amino acids (B). A 2D interaction diagram of **ISB1**-MAO-B complex (C). Protein–ligand contact analysis of the MD trajectory (D). In panel (A), the RMSD of protein and **ISB1** are depicted in blue and red, respectively.

the dried products were recrystallized (Fig. 2). Employing the solvent system hexane : ethyl acetate (2 : 1), thin layer chromatography (TLC) was performed on pre-coated TLC plates (silica gel 60-120#) to monitor all of the reactions.

Chemicals

For synthesis, isatin derivatives and hydrazine hydrate were purchased from Sigma-Aldrich (St. Louis, MO, USA) and TCI chemical. Substrates (benzylamine and kynuramine) and reference inhibitors (clorgyline, lazabemide, pargyline, and toloxatone) as well as recombinant human MAO-A and MAO-B were purchased from Sigma-Aldrich. For reversibility test was performed by using Dialyzer 6–8 kDa DiaEasy™ (BioVision, St. Grove, MA, USA).

Inhibition studies of MAO-B and MAO-A

The MAO-B and MAO-A activities were evaluated using and 0.3 mM benzylamine and 0.06 mM kynuramine, respectively.[61] The previously reported continuous assay method (MAO-A at 316 nm and MAO-B at 250 nm) was used to determine the absorbance.[62] The inhibition of the compounds was compared to that of the reference inhibitors of MAO-A (toloxatone and clorgyline) and MAO-B (lazabemide and pargyline). Utilizing version 5 of the GraphPad Prism software, the compounds' IC_{50} values were determined.[63] The selectivity indices (SI) of the compounds were estimated by: (IC_{50} of MAO-A)/(IC_{50} of MAO-B).[64]

Enzyme kinetics

The inhibition types of the **ISB1** and **ISFB1** lead compounds for MAO-B were determined at five distinct substrate concentrations (0.0375–0.60 μM benzylamine for MAO-B),[61,65] and at three different inhibitor concentrations that were 0.5, 1.0, and 1.5 times their IC_{50} values.[63] By comparing Lineweaver–Burk plots and their secondary plots, the patterns of enzyme inhibition and the K_i values were determined.[62]

Reversibility studies

By comparing the residual activities of dialyzed and undialyzed samples, the reversibility for MAO-B inhibition was determined for lead compounds **ISB1** and **ISFB1** at a concentration of approximately 2.0-times the IC_{50} value after 30 min incubation, as previously described.[61,65] The activities of the compounds were juxtaposed with those of the reference drugs lazabemide and pargyline, which are reversible and irreversible inhibitors of MAO-B, respectively. The reversibility patterns were determined by comparing the activities of the undialyzed (A_U) and dialyzed (A_D) compounds.[61,65]

BBB permeability study

The parallel artificial membrane permeation assay (PAMPA) method was first used in drug research to predict the passive transcellular penetration of pharmaceuticals over the BBB. Using a previous technique developed by our lab, the PAMPA test was carried out on 96-well microtiter and Millipore filter plates with 0.45 micron-sized pores and 125 microns thick (ipvh). The drug concentrations in the receiver, donor and reference wells were determined using UV spectroscopy. The penetration rate was calculated using the formula below.[35,66]

$$\log \mathrm{Pe} = -\ln[1 - C_A/_{\mathrm{equilibrium}}]/A \times (1/V_D + 1/V_A) \times t.$$

Effect of ISB1 on rotenone-induced cell viability

The neuroprotective effect of **ISB1** on rotenone-induced SH-SY5Y cells was analyzed by MTT assay. The cell line was cultured in two 25 cm-tissue culture flasks with DMEM (Sigma-Aldrich, D5648) supplemented with 10% FBS (Gibco, US Origin), L-glutamine (Sigma-Aldrich, G3126), sodium bicarbonate, and antibiotic solution. Cultured cell lines were kept at 37 °C in a humidified 5% CO_2 incubator (NBS Eppendorf, Germany). In 96-well plates, SH-SY5Y cells (5×10^4 cells per well) were cultivated. Cells were pre-treated with rotenone (10 μM) (Sigma-Aldrich, R-8875) at different concentrations in the presence or absence of **ISB1** (1.5, 3.1, 6.25, 12.5, 25 μg in 500 μl of 5% DMEM). After 24 h of incubation, the sample material in wells was removed and 30 μl of reconstituted MTT (Sigma-Aldrich, M-5655) solution was added. After 4 h of incubation at 37 °C in a humidified 5% CO_2 incubator, the supernatant was removed and 100 μl of MTT solubilization solution (DMSO) was added to solubilize the formazan crystals. At a wavelength of 540 nm, the absorbance values were measured using a microplate reader (Erba Lisa Scan EM, Mannheim, Germany).[67]

Molecular docking

Using a *in silico* technique, the binding affinities of **ISB1** and **ISFB1** to the binding sites of human MAO-B with PDB ID:2V5Z were identified. The three-step Protein Preparation Wizard (PPW) was utilized to generate the protein crystal structures, including the program's pre-processing, optimization, and protein energy minimization steps.[68,69] LigPrep was employed during the ligand preparation for docking studies.[70] Receptor grid generation module to grid file was generated at the site of the co-crystallized ligand. Ligand docking was performed in Extra Precision mode (XP).

Molecular dynamic (MD) simulation

By docking poses, the lead molecule **ISB1**, in the hMAO-B enzyme with the least negative score (*e.g.*, the top-docking poses), was the subject of molecular dynamics (MD) research utilizing Desmond in NVIDIA Quadro 6000 graphics processing unit.[71–73] In order to construct trajectories of 1000 frames each to explore interactions between protein and ligand, the default parameter was employed for the systems under research. This included 100 ns MD generation with coordinates recorded at 100 ps. According to previous studies, additional data for MD investigations including box type, estimates of long- and short-range interactions, thermostat and barometer settings, were taken into consideration.[74–78] Finally, stability analysis was performed by employing a tool for simulating interaction diagrams.

Conclusions

Novel classes of eighteen isatin-based benzyloxybenzaldehyde derivatives were synthesized, and their effectiveness in inhibiting MAOs was tested. The lead molecules (3*Z*)-3-((4-(benzyloxy) benzylidene)hydrazineylidene)indolin-2-one (**ISB1**) and (3*Z*)-3-((4-((3-fluorobenzyl)oxy)benzylidene)hydrazineylidene)indolin-2-one (**ISFB1**) exhibited potent MAO-B inhibitory activity with IC_{50} values of 0.124 ± 0.007 and 0.135 ± 0.002 μM, respectively. The leading compounds **ISB1** and **ISFB1** appeared to be competitive MAO-B inhibitors with the K_i values of 0.055 ± 0.010 and 0.069 ± 0.025 μM, respectively. The reversible mode of MAO-B inhibition and the BBB permeation nature of the lead molecules also claimed its CNS-drug likeness. Finally, the present study revealed that **ISB1** significantly reduced rotenone-induced cell death in SH-SY5Y neuroblastoma cells. The docking and simulation studies indicated a pi–pi stacking interaction in the phenyl ring of isatin and hydrogen bonding formed by the imino nitrogen in **ISB1** that maintained the stability of the protein–ligand complex. In short, our findings imply that **ISB1** and **ISFB1** are considered to be candidate agents for the treatment of PD based on the reversible inhibition of MAO-B.

Author contributions

Conceptualization, B. M. and H. K.; synthesis, F. B., S. K., M. M. G., and M. S. A. B.; biological tests, J. M. O. and M. A. A.; docking simulation, N. K. and J. J.; writing—original draft preparation, F. B., J. M. O., and S. K.; writing—review and editing, B. M. and H. K.; supervision, B. M. and H. K.; funding acquisition, H. K. All authors have read and agreed to the published version of the manuscript.

Conflicts of interest

There are no conflicts of interest to declare.

Acknowledgements

The authors are thankful to AlMaarefa University for their support. This study was supported by the National Research Foundation of Korea (NRF) grant funded by the Korea government (NRF-2022R1A2B5B01002536).

References

1 L. M. de Lau and M. M. Breteler, *Lancet Neurol.*, 2006, **5**, 525–535.
2 D. Robakis and S. Fahn, *CNS Drugs*, 2015, **29**, 433–441.
3 P. Maiti, J. Manna and G. L. Dunbar, *Transl. Neurodegener.*, 2017, **6**, 28.
4 N. Eriksen, A. K. Stark and B. Pakkenberg, in *Birth, Life and Death of Dopaminergic Neurons in the Substantia Nigra*, Springer Vienna, Vienna, 2009, pp. 203–213.
5 J. Zheng, X. Zhang and X. Zhen, *ACS Chem. Neurosci.*, 2019, **10**, 783–791.
6 G. Gao, Z. Wang, L. Lu, C. Duan, X. Wang and H. Yang, *Biomed. Pharmacother.*, 2017, **96**, 1380–1388.
7 N. Plotegher, G. Berti, E. Ferrari, I. Tessari, M. Zanetti, L. Lunelli, E. Greggio, M. Bisaglia, M. Veronesi, S. Girotto, M. Dalla Serra, C. Perego, L. Casella and L. Bubacco, *Sci. Rep.*, 2017, **7**, 40699.
8 Y.-Y. Tan, P. Jenner and S.-D. Chen, *J. Parkinson's Dis.*, 2022, **12**, 477–493.

9 J. C. Shih, *J. Neural Transm.*, 2018, **125**, 1553–1566.
10 M. Bortolato, K. Chen and J. C. Shih, *Adv. Drug Delivery Rev.*, 2008, **60**, 1527–1533.
11 C. J. Fowler, A. Wiberg, L. Oreland, J. Marcusson and B. Winblad, *J. Neural Transm.*, 1980, **49**, 1–20.
12 S. Carradori, M. D'Ascenzio, P. Chimenti, D. Secci and A. Bolasco, *Mol. Diversity*, 2014, **18**, 219–243.
13 J. Y. Heo, M.-H. Nam, H. H. Yoon, J. Kim, Y. J. Hwang, W. Won, D. H. Woo, J. A. Lee, H.-J. Park, S. Jo, M. J. Lee, S. Kim, J.-E. Shim, D.-P. Jang, K. I. Kim, S. H. Huh, J. Y. Jeong, N. W. Kowall, J. Lee, H. Im, J. H. Park, B. K. Jang, K. D. Park, H. J. Lee, H. Shin, I.-J. Cho, E. M. Hwang, Y. Kim, H. Y. Kim, S.-J. Oh, S. E. Lee, S. H. Paek, J. H. Yoon, B. K. Jin, G. R. Kweon, I. Shim, O. Hwang, H. Ryu, S. R. Jeon and C. J. Lee, *Curr. Biol.*, 2020, **30**, 276–291e9.
14 J. J. Chen and D. M. Swope, *J. Clin. Psychopharmacol.*, 2005, **45**, 878–894.
15 H. Juárez Olguín, D. Calderón Guzmán, E. Hernández García and G. Barragán Mejía, *Oxid. Med. Cell. Longevity*, 2016, **2016**, 1–13.
16 H. H. Chan, M. K. Tse, S. Kumar and L. Zhuo, *Eur. J. Pharmacol.*, 2018, **818**, 254–262.
17 B. Mathew, J. M. Oh, M. A. Abdelgawad, A. Khames, M. M. Ghoneim, S. Kumar, L. R. Nath, S. T. Sudevan, D. G. T. Parambi, C. Agoni, M. E. S. Soliman and H. Kim, *ACS Omega*, 2022, **7**, 8184–8197.
18 S. Carradori and R. Silvestri, *J. Med. Chem.*, 2015, **58**, 6717–6732.
19 S. Perez-Lloret and O. Rascol, *Expert Rev. Neurother.*, 2016, **16**, 245–258.
20 L. Dézsi and L. Vécsei, *Expert Opin. Invest. Drugs*, 2014, **23**, 729–742.
21 P. Sanchez Alonso, B. De La Casa-Fages, A. Alonso-Cánovas and J. C. Martínez-Castrillo, *Brain Sci.*, 2023, **13**, 276.
22 T. Müller, *Neurodegener. Dis. Manage.*, 2020, **10**, 195–204.
23 S. T. Sudevan, T. M. Rangarajan, A. G. Al-Sehemi, A. S. Nair, V. P. Koyiparambath and B. Mathew, *Arch. Pharm.*, 2022, **355**, 2200084.
24 B. Mathew, S. Carradori, P. Guglielmi, M. S. Uddin and H. Kim, *Curr. Med. Chem.*, 2020, **28**, 266–283.
25 F. Mazouz, S. Gueddari, C. Burstein, D. Mansuy and R. Milcent, *J. Med. Chem.*, 1993, **36**, 1157–1167.
26 M. Naoi and K. Yagi, *Arch. Biochem. Biophys.*, 1980, **205**, 18–26.
27 V. Pérez, J. L. Marco, E. Fernández-Álvarez and M. Unzeta, *Br. J. Pharmacol.*, 1999, **127**, 869–876.
28 S. Kumar, A. S. Nair, M. A. Abdelgawad and B. Mathew, *ACS Omega*, 2022, **7**, 16244–16259.
29 M. Fabbri, M. M. Rosa, D. Abreu and J. J. Ferreira, *Neurodegener. Dis. Manage.*, 2015, **5**, 481–496.
30 M. Joy, B. Mathew and C. Sudarsanakumar, *Chem. Data Collect.*, 2018, **17–18**, 404–414.
31 C. Binda, J. Wang, L. Pisani, C. Caccia, A. Carotti, P. Salvati, D. E. Edmondson and A. Mattevi, *J. Med. Chem.*, 2007, **50**, 5848–5852.
32 F. Leonetti, C. Capaldi, L. Pisani, O. Nicolotti, G. Muncipinto, A. Stefanachi, S. Cellamare, C. Caccia and A. Carotti, *J. Med. Chem.*, 2007, **50**, 4909–4916.
33 I. Bolea, J. Juárez-Jiménez, C. de los Ríos, M. Chioua, R. Pouplana, F. J. Luque, M. Unzeta, J. Marco-Contelles and A. Samadi, *J. Med. Chem.*, 2011, **54**, 8251–8270.
34 I. Bolea, M. A. Colivicchi, C. Ballini, J. Marco-Contelles, K. F. Tipton, M. Unzeta and L. Della Corte, *CNS Neurosci. Ther.*, 2014, **20**, 641–650.
35 S. T. Sudevan, J. M. Oh, M. A. Abdelgawad, M. A. S. Abourehab, T. M. Rangarajan, S. Kumar, I. Ahmad, H. Patel, H. Kim and B. Mathew, *Sci. Rep.*, 2022, **12**, 22404.
36 R. I. Al-Wabli, A. A. Almomen, M. S. Almutairi, A. B. Keeton, G. A. Piazza and M. I. Attia, *Drug Des., Dev. Ther.*, 2020, **14**, 483–495.
37 P. K. Shukla, M. P. Singh and R. Patel, *J. Appl. Pharm. Sci. Res.*, 2018, **1**, 16–22.
38 D. Bonivento, E. M. Milczek, G. R. McDonald, C. Binda, A. Holt, D. E. Edmondson and A. Mattevi, *J. Biol. Chem.*, 2010, **285**, 36849–36856.
39 M. Tavari, S. F. Malan and J. Joubert, *MedChemComm*, 2016, **7**, 1628–1639.
40 F. Hubálek, C. Binda, A. Khalil, M. Li, A. Mattevi, N. Castagnoli and D. E. Edmondson, *J. Biol. Chem.*, 2005, **280**, 15761–15766.
41 C. Liang, J. Xia, D. Lei, X. Li, Q. Yao and J. Gao, *Eur. J. Med. Chem.*, 2014, **74**, 742–750.
42 K. Kopka, A. Faust, P. Keul, S. Wagner, H.-J. Breyholz, C. Höltke, O. Schober, M. Schäfers and B. Levkau, *J. Med. Chem.*, 2006, **49**, 6704–6715.
43 Q. Zhang, Y. Fu, Y. Zhao, S. Cui, J. Wang, F. Liu, Y. Yuan, H. Galons, P. Yu and Y. Teng, *RSC Adv.*, 2019, **9**, 36690–36698.
44 P. Pakravan, S. Kashanian, M. M. Khodaei and F. J. Harding, *Pharmacol. Rep.*, 2013, **65**, 313–335.
45 F. D. Popp, R. Parson and B. E. Donigan, *J. Pharm. Sci.*, 1980, **69**, 1235–1237.
46 S. N. Pandeya, S. Smitha, M. Jyoti and S. K. Sridhar, *Acta Pharm.*, 2005, **55**, 27–46.
47 V. Varun, S. Sonam and R. Kakkar, *MedChemComm*, 2019, **10**, 351–368.
48 J. L. Hyatt, T. Moak, M. J. Hatfield, L. Tsurkan, C. C. Edwards, M. Wierdl, M. K. Danks, R. M. Wadkins and P. M. Potter, *J. Med. Chem.*, 2007, **50**, 1876–1885.
49 R. Nath, S. Pathania, G. Grover and M. J. Akhtar, *J. Mol. Struct.*, 2020, **1222**, 128900.
50 T. R. Bal, B. Anand, P. Yogeeswari and D. Sriram, *Bioorg. Med. Chem. Lett.*, 2005, **15**, 4451–4455.
51 M. S. Vishnu, V. Pavankumar, S. Kumar and A. S. Raja, *ChemMedChem*, 2019, **14**, 1359–1376.
52 E. M. Milczek, C. Binda, S. Rovida, A. Mattevi and D. E. Edmondson, *FEBS J.*, 2011, **278**, 4860–4869.
53 G. E. Mathew, J. M. Oh, K. Mohan, A. Tengli, B. Mathew and H. Kim, *J. Biomol. Struct. Dyn.*, 2021, **39**, 4786–4794.

54 B. Mathew, J. M. Oh, R. S. Baty, G. E.-S. Batiha, D. G. T. Parambi, N. Gambacorta, O. Nicolotti and H. Kim, *Environ. Sci. Pollut. Res.*, 2021, **28**, 38855–38866.
55 Y. Boulaamane, I. Ahmad, H. Patel, N. Das, M. R. Britel and A. Maurady, *J. Biomol. Struct. Dyn.*, 2023, **41**, 2326–2340.
56 D. Osmaniye, Ş. Karaca, B. Kurban, M. Baysal, I. Ahmad, H. Patel, Y. Özkay and Z. Asım Kaplancıklı, *Bioorg. Chem.*, 2022, **122**, 105709.
57 S. Ghosh, S. Das, I. Ahmad and H. Patel, *J. Indian Chem. Soc.*, 2021, **98**, 100272.
58 U. Acar Çevik, I. Celik, A. Işık, I. Ahmad, H. Patel, Y. Özkay and Z. A. Kaplancıklı, *J. Biomol. Struct. Dyn.*, 2023, **41**, 1944–1958.
59 R. Zrieq, I. Ahmad, M. Snoussi, E. Noumi, M. Iriti, F. D. Algahtani, H. Patel, M. Saeed, M. Tasleem, S. Sulaiman, K. Aouadi and A. Kadri, *Int. J. Mol. Sci.*, 2021, **22**, 10693.
60 Y. O. Ayipo, I. Ahmad, Y. S. Najib, S. K. Sheu, H. Patel and M. N. Mordi, *J. Biomol. Struct. Dyn.*, 2023, **41**, 1959–1977.
61 H. W. Lee, H. W. Ryu, M.-G. Kang, D. Park, S.-R. Oh and H. Kim, *Bioorg. Med. Chem. Lett.*, 2016, **26**, 4714–4719.
62 J. M. Oh, H.-J. Jang, W. J. Kim, M.-G. Kang, S. C. Baek, J. P. Lee, D. Park, S.-R. Oh and H. Kim, *Int. J. Biol. Macromol.*, 2020, **151**, 441–448.
63 J. M. Oh, Y. Kang, J. H. Hwang, J.-H. Park, W.-H. Shin, S.-K. Mun, J. U. Lee, S.-T. Yee and H. Kim, *Int. J. Biol. Macromol.*, 2022, **217**, 910–921.
64 S. C. Baek, M. H. Park, H. W. Ryu, J. P. Lee, M.-G. Kang, D. Park, C. M. Park, S.-R. Oh and H. Kim, *Bioorg. Chem.*, 2019, **83**, 317–325.
65 H. W. Lee, H. W. Ryu, M.-G. Kang, D. Park, H. Lee, H. M. Shin, S.-R. Oh and H. Kim, *Int. J. Biol. Macromol.*, 2017, **97**, 598–605.
66 L. Di, E. H. Kerns, K. Fan, O. J. McConnell and G. T. Carter, *Eur. J. Med. Chem.*, 2003, **38**, 223–232.
67 S. Pakrashi, J. Chakraborty and J. Bandyopadhyay, *Neurochem. Res.*, 2020, **45**, 1962–1973.
68 N. C. Desai, A. S. Maheta, A. M. Jethawa, U. P. Pandit, I. Ahmad and H. Patel, *J. Heterocycl. Chem.*, 2022, **59**, 879–889.
69 B. Chaudhari, H. Patel, S. Thakar, I. Ahmad and D. Bansode, *In Silico Pharmacol.*, 2022, **10**, 10.
70 R. Girase, I. Ahmad, R. Pawara and H. Patel, *SAR QSAR Environ. Res.*, 2022, **33**, 215–235.
71 N. C. Desai, S. B. Joshi, A. G. Khasiya, D. J. Jadeja, H. K. Mehta, M. Pandya, I. Ahmad and H. Patel, *J. Mol. Struct.*, 2022, **1270**, 134000.
72 D. Osmaniye, Ş. Karaca, B. Kurban, M. Baysal, I. Ahmad, H. Patel, Y. Özkay and Z. Asım Kaplancıklı, *Bioorg. Chem.*, 2022, **122**, 105709.
73 I. Ahmad, R. Pawara and H. Patel, *Mol. Simul.*, 2022, **48**, 1639–1649.
74 H. A. Radwan, I. Ahmad, I. M. M. Othman, M. A. M. Gad-Elkareem, H. Patel, K. Aouadi, M. Snoussi and A. Kadri, *J. Mol. Struct.*, 2022, **1264**, 133312.
75 M. M. Farhan, M. A. Guma, M. A. Rabeea, I. Ahmad and H. Patel, *J. Mol. Struct.*, 2022, **1269**, 133781.
76 U. Acar Çevik, I. Celik, A. Işık, I. Ahmad, H. Patel, Y. Özkay and Z. A. Kaplancıklı, *J. Biomol. Struct. Dyn.*, 2023, **41**, 1944–1958.
77 M. S. Tople, N. B. Patel, P. P. Patel, A. C. Purohit, I. Ahmad and H. Patel, *J. Mol. Struct.*, 2023, **1271**, 134016.
78 I. Ahmad, R. H. Pawara, R. T. Girase, A. Y. Pathan, V. R. Jagatap, N. Desai, Y. O. Ayipo, S. J. Surana and H. Patel, *ACS Omega*, 2022, **7**, 21820–21844.